Precise control of the degree and regioselectivity of functionalization in nitro- and amino-functionalized di(trispyrazolylborato)iron(II) spin crossover complexes

*Chenyang Ma, Claire Besson**

Department of Chemistry, The George Washington University, 800 22nd Street NW, Washington, D.C. 20052, United States

ABSTRACT:

Di(trispyrazolylborato)iron(II) ([Tp_2Fe]) complexes represent one of the most robust class of spin crossover complexes. Their stability renders them particularly suitable for integration in nanoscale devices, e.g. as sensors or information storage units. While prior studies of the functionalization of those derivatives have been focused on the electronic and steric effect of alkyl and -CF_3 groups in position 3, a pyrazole exchange reaction between nitropyrazole and either trispyrazolylborate or its iron complex allows the regioselective installation of nitro substituents in positions 3, 4 and 5 of [Tp_2Fe] complexes. The degree of substitution can be varied from 1 to 4 functionalized pyrazoles per complex. The amine functionalized analogues are accessed by reduction of the nitro analogues under hydrogen transfer conditions. With the exception of di- and tetra-3-NO_2 substituted complexes, all derivatives display spin crossover properties in the solid state, with transition temperatures ranging from 180 to 380 K and showing

different degree of abruptness, but no hysteresis. The Slichter-Drickamer model was used to extract empirical thermodynamic transition parameters, allowing a systematic investigation of the influence of stoichiometry, position, and electronic nature of the substitution on the magnetic properties of the complexes. Steric effects dominate for substitution in position 3, but electronic effects are significant for the other positions.

INTRODUCTION

Spin crossover complexes are transition metal complexes, with electronic configurations d^4 to d^7, which can be reversibly switched between two different (meta)stable spin states by applying an external physical stimulus, e.g. temperature, pressure, or light.[1, 2] They have attracted significant attention for their potential as sensors, information storage and processing units and displays.[3-5] Also, spin crossover materials with both abrupt transitions and hysteresis loops[6-8] are ideal candidates for molecular switches and data storage.[9-12] However, effective engineering of spin crossover properties remains a challenge.[13] The most common approach is substitution at the ligand backbone, which can impact the spin crossover through electronic and/or steric effects. For example, Damrauer and Aromí have shown that substitution of polypyridine or bispyrazolylpyridine ligands close to the metal center favors the high-spin states of the complexes through an essentially steric effect.[14-20] In bispyrazolypyridine and other related systems, remote substitution by electron withdrawing group was revealed to stabilize the low spin states of the complexes, while electron donating groups stabilize the high spin states.[16, 21-28] Another key challenge for the implementation of spin crossover materials is the relative fragility of the crossover properties and the complexes that display them.[8, 29] In that context, trispyrazolylborate (Tp^-) complex of iron(II) are particularly attractive. The archetypal [$FeTp_2$]

complex, discovered in 1967[30, 31] and extensively studied since then,[32-36] exemplifies the robust spin crossover properties and remarkable stability under light, electromagnetic fields, air and water which are characteristic of this family of compounds. Multiple reports have shown the impact of substitution at the pyrazole rings or at the boron on the spin crossover properties,[27, 28, 37-46] achieving transition temperatures $T_{1/2}$ ranging from 85 K for [{(3-Me-pz)$_3$BH}$_2$Fe][27] to 365 K for the unsubstituted complex.[35] Most of those studies, however, have been limited to complexes with six identical pyrazoles, and have concentrated on the steric effects of substitution in position 3 (closer to the metal). We recently demonstrated the controlled exchange of one or two 4-nitropyrazoles into trispyrazolylborate to form mono- or dinitrated trispyrazolylborate ligands. The resulting iron(II) complexes achieve spin transition temperatures above 400 K,[47] suggesting electronic control of the spin crossover is possible in trispyrazolyborateiron complexes.

The present article investigates the key parameters controlling the pyrazole exchange reaction and shows how it can be applied for the synthesis of trispyrazolylborate complexes functionalized in positions 3, 4 and 5. We also demonstrate the synthesis of heteroleptic complexes. These results allow us to provide a systematic investigation of the influence of stoichiometry, position and electronic nature of the substitution on the solid state structural and magnetic properties of di(trispyrazolylborato)iron(II) complexes, thus gaining a detailed insight on the interplay of electronic and steric effects.

EXPERIMENTAL SECTION

While we have not observed any dangerous behavior so far for any of the compounds reported here, nitropyrazoles are nitrogen- and oxygen-rich derivatives with potential explosive qualities and should be handled with precaution. All reagents and solvents were purchased from

commercial sources and utilized as received. Di(trispyrazolyborato)iron ([Tp_2Fe]) was synthesized as described by Trofimenko.[30] 3(5)-nitropyrazole,[48, 49] 4-nitropyrazole, [50, 51] and tetrabutylammonium trispyrazolyborate (TBATp) [52] were prepared according to the literature. All reactions are performed under dry nitrogen using standard Schlenk techniques.

Instrumentation. Elemental analyses were performed by ALS Environmental, except [(Tp)Fe(3-NO_2Tp)]·(C_6H_6)$_{0.5}$ and [(Tp)Fe(5-NO_2Tp)], where the iron content were determined on a Shimadzu simultaneous inductively coupled plasma atomic emission spectrometry (ICPE-9800) using samples were dissolved in 6 ml aqua regia, then diluted to 50 ml with DI water and a calibration curve (r = 0.99825) constructed from four $Fe(NO_3)_3$ standard solutions at iron concentrations 2.935, 14.67, 29.35 and 58.70 mg/L. Electronic absorption spectra were recorded with a Shimadzu UV 2401PC spectrophotometers or SPECORD S 600 UV Vis Diode-array Spectrophotometer. FTIR spectra were obtained in transmission mode using a Perkin–Elmer Frontier FTIR Spectrometer with samples diluted in KBr pellets. Single crystals were selected from the bulk samples and mounted on MiTeGen MicroMounts. Reflection data were collected at 100 K or 298.15 K with 0.5° ω and φ scans on a Bruker SMART diffractometer equipped with an APEX II CCD detector using MoKα (λ = 0.71073 Å) radiation. Powder X-ray diffraction (PXRD) data were collected on a Rigaku Miniflex (Cu Kα 2θ = 3 – 60) and baseline corrected using the Fityk software program. Crystalline samples for SQUID magnetometry were dried under vacuum at 100°C for 4 hours and then enclosed in a copper foil pouch and mounted on a quartz holder with kapton tape (T < 300 K) or directly on the heater stick (T > 300K). Data was collected at 0.1 T with a Quantum Design SQUID MPMS3 magnetometer. The molar diamagnetic susceptibility of the compounds was estimated from their molar mass (χ_{dia} (cm^3/mol) = - [MW(g/mol)×10^{-6}]/2) and subtracted from the experimental value. PXRD data was collected

from all samples after the SQUID measurements, showing that [(Tp)Fe(3-NO_2Tp)]·$(C_6H_6)_{0.5}$, [(Tp)Fe(4-NO_2Tp)], [(3-NO_2Tp)$_2$Fe], [((3-NO_2)$_2$Tp)$_2$Fe], [(3-NH_2Tp)$_2$Fe] and [((3-NH_2)$_2$Tp)$_2$Fe] retained their original structure while [(Tp)Fe(5-NO_2Tp)]·$(CH_3CN)_{0.5}$ and [((3-NO_2)$_2$Tp)$_2$Fe]·CH_2Cl_2 lost their solvent while retaining crystallinity. The pKa of 3-nitropyrazole and 4-nitropyrazole were determined by titrating a solution containing 3-nitropyrazole or 4-nitropyrazole (0.0312 M) and acid (HCl 0.04 M) with a NaOH solution (0.05 M) and fitting the resulting curve using CurTipot.[53]

Synthesis.

^{n}Bu$_4$N[HB(4-NO_2pz)(pz)$_2$]. ^{n}Bu$_4$NTp (1.00 g, 2.20 mmol, 1.00 eq.) and 4-nitro-1*H*-pyrazole (0.248 g, 2.20 mmol, 1.00 eq) were mixed in a Schlenk tube and heated to 90°C for 4 h. Solid pyrazole condensed on the side of the tube was removed at one-hour intervals. The crude product was washed with 10 mL water, then dried under vacuum, yielding the product as a white solid (0.77 g, 1.54 mmol, 70%). Single crystals suitable for X-ray analysis were obtained from a saturated solution in chloroform layered with diethyl ether. Spectroscopic data matches previously reported characterizations. [47]

^{n}Bu$_4$N[HB(3-NO_2pz)(pz)$_2$]. ^{n}Bu$_4$NTp (1.00 g, 2.20 mmol, 1.00 eq.) and 3-nitro-1*H*-pyrazole (0.248 g, 2.20 mmol, 1.00 eq) were mixed in a Schlenk tube and heated in an oil bath at 105°C for 4 h. Solid pyrazole condensed on the side of the tube was removed at one-hour intervals. The crude product was washed with 10 mL water, then dried under vacuum, yielding the product as a white solid (0.77 g, 1.54 mmol, 70%). Single crystals suitable for X-ray analysis were obtained from a saturated solution in chloroform layered with diethyl ether. ^{1}H-NMR (400 MHz, DMSO-d_6, 300 K): δ nm= 7.45 (d, J = 2.1 Hz, 2H), 7.40 (d, J = 1.6 Hz, 2H), 7.29 (d, J = 2.4 Hz, 1H),

6.75 (d, *J* = 2.4 Hz, 1H), 6.08 (t, *J* = 1.8 Hz, 2H), 3.20-3.11 (m, 8H), 1.62-1.51 (m, 8H), 1.30 (sext, *J* = 7.3 Hz, 8H), 0.93 (t, *J* = 7.3 Hz, 12H). IR (KBr, cm^{-1}): ν = 2963 (m), 2876 (m), 2451.5 (m, B-H), 1526.5 (s), 1490.5 (vs), 1382 (vs), 1364.5 (vs), 1291.5 (s), 1224 (s), 1151 (vs), 1098 (vs), 1037 (m).

$^{n}Bu_4N[HB(3\text{-}NO_2pz)_2(pz)]$. $^{n}Bu_4NTp$ (0.50 g, 1.10 mmol, 1.00 eq.) and 3-nitro-1*H*-pyrazole (0.248 g, 2.20 mmol, 2.00 eq) were mixed in a Schlenk tube and heated to 130 °C for 4 h. Pyrazole sublimated on the side of the tube was removed at one-hour intervals. The reaction gave a yellow liquid in almost quantitative yield. The crude product was used without further purification. ^{1}H-NMR (400 MHz, DMSO-d_6, 300 K): δ nm= 7.57 (d, *J* = 2.2 Hz, 1H), 7.52 (d, *J* = 2.4 Hz, 2H), 7.49 (d, *J* = 1.5 Hz, 1H), 6.83 (d, *J* = 2.4 Hz, 2H), 6.16 (t, *J* = 1.92 Hz, 1H), 3.20-3.11 (m, 8H), 1.62-1.51 (m, 8H), 1.30 (sext, *J* = 7.3 Hz, 8H), 0.93 (t, *J* = 7.3 Hz, 12H). IR (ATR, cm^{-1}): ν = 2963.5 (m), 2876 (m), 2454.5 (m, B-H), 1527 (s), 1491.5 (vs), 1381 (s), 1365 (vs), 1294.5 (s), 1225 (s), 1151.5 (vs), 1103 (vs), 1052.5 (m).

[(3-NO_2Tp)$_2$Fe]. To a vigorously stirred solution of $^{n}Bu_4N$ [HB(3-NO_2pz)(pz)$_2$] (1.30 g, 2.60 mmol, 2.00 eq.) in DCM (70 mL) was added $FeCl_2 \cdot 4H_2O$ (0.258 g, 1.30 mmol, 1.00 eq.). The solution instantly turned dark brown. After heating at reflux for 1 h the solvent was removed under reduced pressure. The resulting brown solid was suspended in water (80 mL), filtered off and re-dissolved in dichloromethane (50 mL). The dichloromethane solution was then poured through a silica gel plug (3 cm diameter, 3 cm height) and the silica gel plug washed with more dichloromethane until the eluent passing through was clear. The solvent was removed by rotary evaporation, yielding the product as a pinkish yellow solid (0.558 g, 0.975 mmol, 75%). Single crystals suitable for X-ray diffraction were obtained from a saturated solution in

dichloromethane (4 mL) layered with 1 mL dichloromethane then with 15 mL methanol, after 3 days of diffusion (0.351g, 0.614 mmol, 63% yield). ^{1}H-NMR (400 MHz, CD_2Cl_2, 300 K): 51.7 (br, $\Delta\nu_{1/2}$ = 1062.5 Hz), 49.8 (br, $\Delta\nu_{1/2}$ = 128.6 Hz), 48.1 (br, $\Delta\nu_{1/2}$ = 1237.9 Hz), 45.2 (br, $\Delta\nu_{1/2}$ = 130.2 Hz), 43.5 (br, $\Delta\nu_{1/2}$ = 122.9 Hz), 42.5 (br, $\Delta\nu_{1/2}$ = 126.8 Hz), 40.9 (br, $\Delta\nu_{1/2}$ = 1269.4 Hz), 40.0 (br, $\Delta\nu_{1/2}$ = 116.95 Hz), 13.5 (br, $\Delta\nu_{1/2}$ = 205.23 Hz), 9.6 (br, $\Delta\nu_{1/2}$ = 207.85 Hz), 6.6 (br, $\Delta\nu_{1/2}$ = 210.23 Hz), 6.0 (br, $\Delta\nu_{1/2}$ = 208.94 Hz), 4.6 (br, $\Delta\nu_{1/2}$ = 223.3 Hz), -42.5 (br, $\Delta\nu_{1/2}$ = 626.1 Hz). IR (KBr, cm^{-1}): ν = 3137 (m), 2476 (m, B-H), 1542 (s), 1504 (s), 1404 (s), 1389 (m), 1377 (m), 1310 (s), 1220 (s), 1165 (s), 1118 (s), 1070 (m), 1067 (s), 1050 (vs). EA (%): Expected C: 37.80, H: 3.17, N: 34.29, Fe:9.76; Found C: 37.85, H: 3.18, N: 34.17, Fe: 9.42. UV [Toluene; λ_{max}, nm (log ε)]: 439 (1.6).

[(Tp)Fe(3-NO$_2$Tp)]. To a vigorously stirred solution of ^{n}Bu$_4$N[HB(3-NO$_2$pz)(pz)$_2$] (1.26g, 2.52 mmol, 2.00 eq.) and Bu$_4$N[HB(pz)$_3$] (0.575 g, 1.26 mmol, 1.00 eq.) in DCM (80 mL) was added $FeCl_2 \cdot 4H_2O$ (0.368 g, 1.85 mmol, 1.50 eq.). The solution instantly turned dark brown. After heating at reflux for 1 hour, the solvent was removed under reduced pressure. The resulting brown solid was suspended in water (80 mL), filtered off and re-dissolved in dichloromethane (50 mL). The dichloromethane solution was then poured through a silica gel plug (3 cm diameter, 3 cm height) and the silica gel plug washed with more dichloromethane until the eluent passing through was clear. The solvent was removed by rotary evaporation, resulting in a brown solid, which was purified by silica gel column chromatography (CH_2Cl_2/n-hexane = 1/4) to give [(Tp)Fe(3-NO$_2$Tp)] as a blue solid (0.388 g, 0.73 mmol, 58%). Single crystals of [(Tp)Fe(3-NO$_2$Tp)]$\cdot$ $(C_6H_6)_{0.5}$ suitable for X-ray diffraction were obtained from a saturated solution in benzene (3 mL) layered with 1 mL benzene then with hexane (15 mL), after 3 day of diffusion under N_2 gas (0.140 g, 0.26 mmol, 36%). ^{1}H-NMR (400 MHz, $(CD_3)_2CO$, 300 K): 48.4

(br, $\Delta\nu_{1/2}$ = 186.2 Hz), 45.8(br, $\Delta\nu_{1/2}$ = 148.3 Hz), 45.1 (br, $\Delta\nu_{1/2}$ = 1470.0 Hz), 41.7 (br, $\Delta\nu_{1/2}$ = 42.6 Hz), 37.8 (br, $\Delta\nu_{1/2}$ = 83.4 Hz), 10.5 (br, $\Delta\nu_{1/2}$ = 192.7 Hz), 9.6(br, $\Delta\nu_{1/2}$ = 277.6 Hz), 8.7 (br, $\Delta\nu_{1/2}$ = 159.3 Hz), 3.9 (br, $\Delta\nu_{1/2}$ = 249.6 Hz), -38.0 (br, $\Delta\nu_{1/2}$ = 540.4 Hz), -40.9 (br, $\Delta\nu_{1/2}$ = 540.4 Hz). IR (KBr, cm^{-1}): ν = 3151 (m), 2466 (m, B-H), 2459 (m, B-H), 1539 (s), 1502(s), 1404 (vs), 1391 (s), 1364 (m), 1306 (vs), 1221 (s), 1160 (s), 1111 (s), 1050 (vs). EA (%, for [(3-NO_2Tp)FeTp]· $(C_6H_6)_{0.5}$**:** Expected C: 44.57, H: 3.92, N: 32.17, Fe: 9.87; Found C: 42.10, H: 3.85, N: 32.47, Fe: 9.62. UV [Toluene; λ_{max}, nm (log ε)]: 476 (2.1).

[((3-NO_2)$_2$Tp)$_2$Fe]. To a vigorously stirred solution of $^{n}Bu_4N$[HB(3-NO_2pz)$_2$(pz)] (1.09 g, 2.00 mmol, 2.00 eq.) in DCM (50 mL) was added $FeCl_2 \cdot 4H_2O$ (0.199 g, 1.00 mmol, 1.00 eq.) in methanol (10 ml). The resulting dark brown solution was stirred for 1 hour at room temperature before the solvent was removed under reduced pressure. The resulting brown solid was suspended in water (80 mL), filtered off and re-dissolved in dichloromethane (50 mL). The dichloromethane solution was then poured through a silica gel plug (3 cm diameter, 3 cm height) and the silica gel plug was further washed with dichloromethane until the eluent was clear. The solvent was removed by rotary evaporation, yielding the product as a light-yellow solid (0.437 g, 0.66 mmol, 66%). [((3-NO_2)$_2$Tp)$_2$Fe]· CH_2Cl_2 crystals suitable for X-ray diffraction were obtained from slow evaporation of a saturated solution in dichloromethane (0.420 g, 0.635 mmol, 96%). De-solvated [((3-NO_2)$_2$Tp)$_2$Fe] crystals suitable for X-ray diffraction were obtained from drying [((3-NO_2)$_2$Tp)$_2$Fe]· CH_2Cl_2 crystals at room temperature under vacuum. ^{1}H-NMR (400 MHz, CD_2Cl_2, 300 K): 47.2 (br, $\Delta\nu_{1/2}$ = 95.9 Hz), 46.9 (br, $\Delta\nu_{1/2}$ = 873.5 Hz), 43.9 (br, $\Delta\nu_{1/2}$ = 100.5 Hz), 41.9 (br, $\Delta\nu_{1/2}$ = 87.5 Hz), 37.8 (br, $\Delta\nu_{1/2}$ = 93.4 Hz), 34.5 (br, $\Delta\nu_{1/2}$ = 93.5 Hz), 30.0 (br, $\Delta\nu_{1/2}$ = 1011.7 Hz), 11.6 (br, $\Delta\nu_{1/2}$ = 190.3 Hz), 9.3 (br, $\Delta\nu_{1/2}$ = 166.4 Hz), 8.8 (br, $\Delta\nu_{1/2}$ = 278.9 Hz), 2.4 (br, $\Delta\nu_{1/2}$ = 183.7 Hz), -2.8 (br, $\Delta\nu_{1/2}$ = 186.5 Hz), -43.2 (br, $\Delta\nu_{1/2}$

= 542.8 Hz), -45.0 (br, $\Delta\nu_{1/2}$ = 745.8 Hz). IR (KBr, cm^{-1}): ν = 3157 (m), 2922 (m), 2494.5 (m, B-H), 1543 (vs), 1503.5 (vs), 1402 (s), 1383 (s), 1311.5 (vs), 1237.5 (s), 1170.5 (vs), 1115.5 (m), 1053.5 (vs). EA (%): Expected C: 32.66, H: 2.44, N: 33.86, Fe: 8.44; Found C: 32.28, H: 2.44, N: 34.14, Fe: 7.87. UV [Dichloromethane; λ_{max}, nm (log ε)]: 439 (1.0).

[(Tp)Fe(4-NO$_2$Tp)]. To a vigorously stirred solution of $^{n}Bu_4N[HB(4\text{-}NO_2pz)(pz)_2]$ (1.30 g, 2.60 mmol, 4.00 eq.) and $Bu_4N[HB(pz)_3]$ (0.296 g, 0.65 mmol, 1.00 eq.) in DCM (80 mL) was added $FeCl_2 \cdot 4H_2O$ (0.324 g, 1.63 mmol, 2.50 eq.). The dark red solution was heated at reflux for 1 hour. The solvent was removed under reduced pressure, and the resulting solid suspended in water (80 mL), filtered of and washed three times with water (50 mL) and one time with hexane (50 mL) to give a dark red solid. Purified by silica gel column chromatography (toluene/n-hexane = 2/3) yielded the product as a red solid (0.153 g, 0.29 mmol, 45%). Single crystals suitable for X-ray diffraction were obtained from slow evaporation of a saturated solution in toluene (0.148 g, 0.28 mmol, 97%). ^{1}H-NMR (400 MHz, CD_2Cl_2, 300 K): 12.9 (br, $\Delta\nu_{1/2}$ = 136.6 Hz), 11.3 (br, $\Delta\nu_{1/2}$ = 320.4 Hz), 10.9 (br, $\Delta\nu_{1/2}$ = 120.9 Hz), 11.0 (br, $\Delta\nu_{1/2}$ = 39.5 Hz), 10.9 (br, $\Delta\nu_{1/2}$ = 32.8 Hz), 10.5 (br, $\Delta\nu_{1/2}$ = 32.9 Hz), 8.1 (br, $\Delta\nu_{1/2}$ = 31.9 Hz), 7.9 (br, $\Delta\nu_{1/2}$ = 38.0 Hz), 7.8 (br, $\Delta\nu_{1/2}$ = 31.8 Hz), -0.4 (br, $\Delta\nu_{1/2}$ = 343.3 Hz). IR (KBr, cm^{-1}): ν = 3145 (m), 2925 (m), 2516 (m, B-H), 2477 (m, B-H), 1502 (s), 1428 (m), 1407 (vs), 1302 (vs), 1219 (s), 1108 (vs), 1042 (s). EA (%): Expected C: 41.03, H: 3.63, N: 34.56, Fe:10.60; Found C: 41.52, H: 3.60, N: 34.28, Fe: 9.82. UV [Toluene; λ_{max}, nm (log ε)]: 531 (2.1).

[(Tp)Fe(5-NO$_2$Tp)]. To a suspension of 3(5)-nitropyrazole (0.0949 g, 0.84 mmol, 4.00 eq.) in o-xylene (10 mL) was added $[FeTp_2]$ (0.100 g, 0.21 mmol, 1.00 eq.). The purple solution was heated at reflux for 12 hours. The resulting dark purple solution (containing some white

unreacted 3(5)-nitropyrazole solid) was poured through a silica gel plug (1 cm diameter, 1 cm height) and the silica gel plug was washed with toluene until the eluent was clear. The solvent was removed by rotary evaporation to give a dark purple solid, which was purified by silica gel column chromatography (CH_2Cl_2/n-hexane = 1/9) to give the product as a dark blue solid (0.0078 g, 0.0148 mmol, 7.0%). A very small amount of [(Tp)Fe(3-NO_2Tp)] was also obtained and unreacted [Tp_2Fe] (0.072 g, 0.15 mmol, 72%) can be recovered. Single crystals of [(Tp)Fe(5-NO_2Tp)]·$(CH_3CN)_{0.50}$ suitable for X-ray diffraction were obtained from slow evaporation of a saturated solution in acetonitrile (7.4 mg, 0.0141 mmol, 95%). ^{1}H-NMR (400 MHz, CD_3CN, 300 K): 9.4 (br, $\Delta\nu_{1/2}$ = 14.9 Hz), 8.7 (br, $\Delta\nu_{1/2}$ = 61.5 Hz), 8.6 (br, $\Delta\nu_{1/2}$ = 52.4 Hz), 8.4 (br, $\Delta\nu_{1/2}$ = 60.4 Hz), 8.1 (br, $\Delta\nu_{1/2}$ = 11.7 Hz), 8.0 (br, $\Delta\nu_{1/2}$ = 10.0 Hz), 8.0 (br, $\Delta\nu_{1/2}$ = 10.5 Hz), 8.0 (br, $\Delta\nu_{1/2}$ = 10.8 Hz), 3.1 (br, $\Delta\nu_{1/2}$ = 109.4 Hz), 2.7 (br, $\Delta\nu_{1/2}$ = 85.5 Hz). IR (KBr, cm^{-1}): ν = 3141 (m), 2925 (m), 2551 (m, B-H), 2477 (m, B-H), 1536 (s), 1496 (s), 1428 (s), 1401 (vs), 1337 (vs), 1311 (vs), 1217 (s), 1111 (vs), 1043 (vs). EA (%): Expected C: 41.03, H: 3.63, N: 34.56, Fe:10.60; Found C: 43.65, H: 4.31, N: 31.25, Fe: 10.3. UV [Toluene; λ_{max}, nm (log ε)]: 575 (3.3).

[(3-NH_2Tp)$_2$Fe]. To a suspension of [(3-NO_2Tp)$_2$Fe] (0.1000 g, 0.175 mmol, 1.00 eq) in ethanol (3 mL) and Toluene (1 mL) in a 10 ml glass vial were added potassium formate (0.0882 g, 1.05 mmol, 6.00 eq) and Pd/C (0.030 g, 5% Pd). The suspension was heated to 75 °C (P ≈ 5.5 bar) for 1 hour in the microwave. Alternatively, the reaction can be conducted with conventional heating under nitrogen gas with 6 hours reflux. The catalyst was filtered off and the solvent removed by rotary evaporation to give a light purple solid. A final wash with water (50 mL) gave the product as a purple solid (0.0651 g, 0.128 mmol, 73% yield). Single crystals suitable for X-ray diffraction were obtained from slow evaporation of a saturated solution in benzene (0.0425 g,

0.083 mmol, 65% yield). ^{1}H-NMR (400 MHz, CD_2Cl_2, 300 K): 44.4 (br, $\Delta\nu_{1/2}$ = 705.5 Hz), 44.1 (br, $\Delta\nu_{1/2}$ = 113.6 Hz), 43.4 (br, $\Delta\nu_{1/2}$ = 97.8 Hz), 41.9 (br, $\Delta\nu_{1/2}$ = 109.8 Hz), 41.7 (br, $\Delta\nu_{1/2}$ = 818.9 Hz), 40.9 (br, $\Delta\nu_{1/2}$ = 112.9 Hz), 39.4 (br, $\Delta\nu_{1/2}$ = 109.3 Hz), 36.6 (br, $\Delta\nu_{1/2}$ = 747.7 Hz), 27.9 (br, $\Delta\nu_{1/2}$ = 854.6 Hz), 27.0 (br, $\Delta\nu_{1/2}$ = 650.6 Hz), 20.3 (br, $\Delta\nu_{1/2}$ = 727.2 Hz), 9.5 (br, $\Delta\nu_{1/2}$ = 221.7 Hz), 4.9 (br, $\Delta\nu_{1/2}$ = 131.4 Hz), -33.0 (br, $\Delta\nu_{1/2}$ = 513.1 Hz). IR (KBr, cm^{-1}): ν = 3443.5 (m), 3376.5 (m), 2475 (m, B-H), 1605 (m), 1538 (vs), 1507 (s), 1407 (s), 1304.5 (s), 1208.5 (vs), 1112 (s), 1045 (s). EA (%): Expected C: 42.23, H: 4.33, N: 38.30, Fe:10.91; Found C: 43.07, H: 4.50, N: 38.12, Fe: 9.98%. UV [Toluene; λ_{max}, nm (log ε)]: 557 (1.3).

[((3-NH$_2$)$_2$Tp)$_2$Fe]. To a suspension of [((3-NO_2)$_2$Tp)$_2$Fe] (0.1000 g, 0.151 mmol, 1.00 eq) in ethanol (4 mL) and toluene (1 mL) were added potassium formate (0.1764 g, 2.10 mmol, 12.00 eq) and Pd/C (0.030g, 5% Pd). The suspension was heated to 70 °C (P ≈ 5.5 bar) for 1 hour in the microwave. The catalyst was filtered off and the solvent removed by rotary evaporation. A final wash with water (50 mL) gave the product as a white solid (0.081 g, 0.135 mmol, 89% yield). Single crystals suitable for X-ray diffraction were obtained from slow evaporation of a saturated solution in dichloromethane (0.075 g, 0.125 mmol, 93% yield). ^{1}H-NMR (400 MHz, C*D$_3$*CN, 300 K): 53.1 (br, $\Delta\nu_{1/2}$ = 128.7 Hz), 51.6 (br, $\Delta\nu_{1/2}$ = 143.5 Hz), 51.4 (br, $\Delta\nu_{1/2}$ = 125.7 Hz), 50.5 (br, $\Delta\nu_{1/2}$ = 811.0 Hz), 49.1 (br, $\Delta\nu_{1/2}$ = 150.5 Hz), 47.5 (br, $\Delta\nu_{1/2}$ = 121.2 Hz), 45.7 (br, $\Delta\nu_{1/2}$ = 915.3 Hz), 36.2 (br, $\Delta\nu_{1/2}$ = 1071.7 Hz), 28.7 (br, $\Delta\nu_{1/2}$ = 1267.5 Hz), 10.8 (br, $\Delta\nu_{1/2}$ = 230.1 Hz), 4.9 (br, $\Delta\nu_{1/2}$ = 303.1 Hz), -41.0 (br, $\Delta\nu_{1/2}$ = 658.4 Hz). IR (KBr, cm^{-1}): ν = 3427 (m), 3321 (m), 2452 (m, B-H), 1619 (m), 1533 (s), 1511 (s), 1414 (s), 1372 (s), 1303 (s), 1206 (vs), 1108 (s), 1045 (s). EA (%): Expected C: 39.89, H: 4.46, N: 41.35, Fe:10.3; Found C: 40.54, H: 4.49, N: 37.43, Fe: 8.43. UV [Dichloromethane; λ_{max}, nm (log ε)]: 437.5 (1.5).

RESULTS AND DISCUSSION

Synthesis. Nitrofunctionalized trispyrazolylborate ligands $HB(3\text{-}NO_2pz)(pz)_2^-$ ($3\text{-}NO_2Tp^-$) and $HB(3\text{-}NO_2pz)_2(pz)^-$ ($(3\text{-}NO_2)_2Tp^-$) were prepared as tetrabutylammonium salts by direct exchange of 3-nitropyrazole with $^nBu_4NTp$ in solvent-free conditions, as described earlier for the 4-substituted analogues, [47] and with the same selectivity for the formation of the *N*-borates over the *O*-borates (Scheme 1). More than the stoichiometry, the temperature of the reaction is key to controlling the degree of functionalization of the ligand. Monosubstituted $3\text{-}NO_2Tp^-$ is obtained exclusively at an oil bath temperature of 105°C even in the presence of an excess of 3-nitropyrazole and increasing the temperature of the reaction to 130°C is necessary to form disubstituted $(3\text{-}NO_2)_2Tp^-$. Both temperatures are higher than is required for the formation of the

Scheme 1. Synthesis of $[(3\text{-}NO_2Tp)_2Fe]$

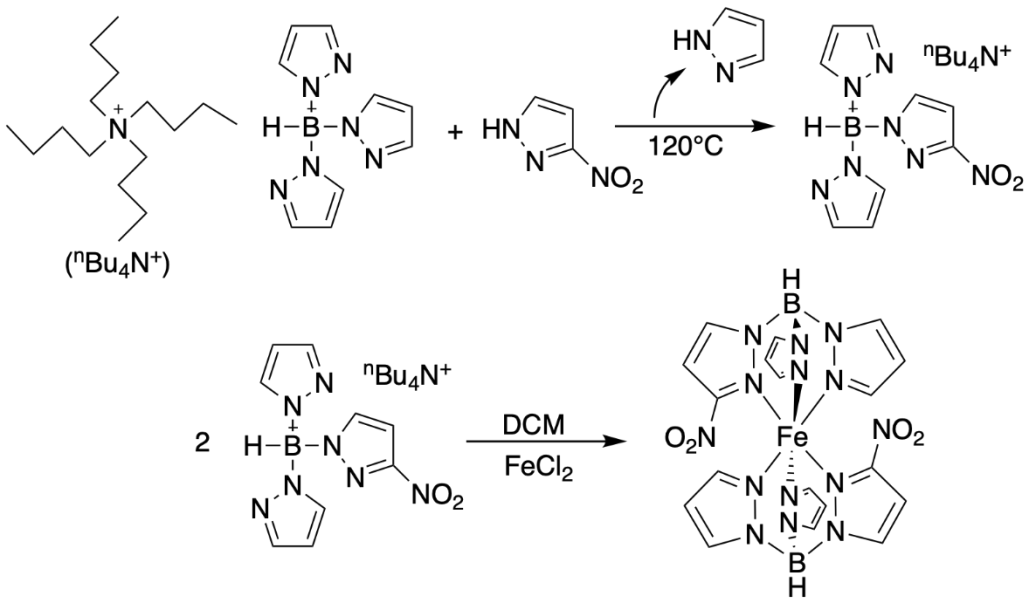

4-nitro analogues (90°C and 125°C, respectively). Those results indicate than the exchange reactions are not simply driven by the distillation of the pyrazole out of the reaction medium. They are, however, in agreement with the HASB theory: the stronger and harder base (pz^- >

3-NO_2pz^-≈4-NO_2pz^-, respective pKa of the pzH, 4-NO_2pzH and 3(5)-NO_2pzH are 14.3,[54] 9.75 and 9.5) binds to the harder acid (H^+ > HBpz(NO_2pz) > $HBpz_2$). Interestingly, the proposed S_N2 mechanism[55, 56] with concerted proton transfer and a transition state characterized by a 6-membered H-N-N…B-N-N… ring (Figure 1),[47] would proceed via the 5-NO_2pzH tautomer of 3(5)-nitropyrazole for the formation of 3 NO_2Tp^-. This tautomer is the minor species in solution at room temperature, which might explain the higher temperature needed for the exchange of

Scheme 2. Synthesis of [(Tp)Fe(5-NO_2Tp)]

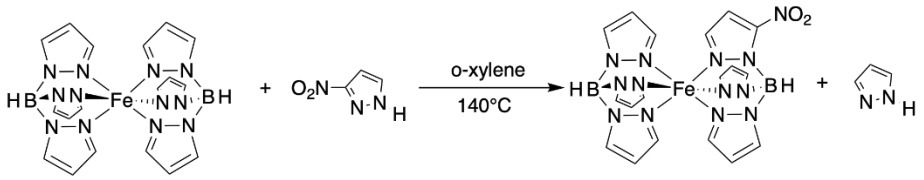

3(5)- vs 4-nitropyrarazole.

The perfect selectivity towards the formation of 3-NO_2Tp^- rather than the 5-substituted analogue is an indication of the strong impact of steric effects on the reaction. We hypothesized that significantly increasing steric hindrance at position 3 would allow the formation of 5-substituted derivatives. Indeed, performing the pyrazole exchange reaction on a complexed Tp^-

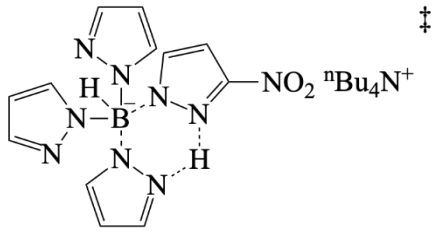

Figure 1. Proposed transition state for 3(5)-nitropyrazole exchange reaction.

ligand (in the form of the $FeTp_2$ complex), where the 5 position is now the most accessible, allowed us to prepare [(Tp)Fe(5-NO_2Tp)], in moderate yield (Scheme 2).

Homoleptic difunctionalized complexes [(3-NO_2Tp)$_2$Fe] and [((3-NO_2)$_2$Tp)$_2$Fe] are formed by the reaction of two equivalents of the appropriate ligand with $FeCl_2$ in DCM at room temperature. Using a mixture of Tp^- and NO_2Tp^- ligands yields the asymmetric monofunctionalized complexes [(Tp)Fe(3-NO_2Tp)] and [(Tp)Fe(4-NO_2Tp)], which can be easily separated from the homoleptic products [Tp_2Fe] and [($NO_2Tp)_2$Fe] by column chromatography. Interestingly, coordination of the ligands is not purely statistic, and homoleptic complexes are significantly favored. Optimal yields of the asymmetric complexes were obtained in non-stoichiometric conditions, with a 4:1 (4-NO_2Tp^-:Tp^-) or 2:1 (3-NO_2Tp^-:Tp^-) ligand ratio reflecting the lower coordination ability of the ligands functionalized with an electron withdrawing group.

Amine-functionalized derivatives are accessible in excellent yields via reduction of the nitro analogues by transfer hydrogenation, using potassium formate or 1,4-cyclohexadiene as hydrogen donor, Pd/C as a catalyst and a protic solvent. This represents a marked improvement in convenience and safety over the conditions (10h reflux under 8 bar H_2) we reported previously for the reduction of the 4-nitro derivatives. Under microwave heating, the reactions can be completed within one hour thanks to the high local temperature afforded by the strong microwave absorptivity of the carbon support. [57, 58]

Despite their very high nitrogen and oxygen content, all complexes are stable in air up to at least 250 °C, as demonstrated by TGA (see Supplementing Information), which shows no mass loss below this temperature except for the occasional loss of crystallization solvent. Preliminary investigations have demonstrated that [(3-NO_2Tp)$_2$Fe] and [(3-NH_2Tp)$_2$Fe] can be sublimated under vacuum without appreciable decomposition.

Single-crystal X-ray diffraction. Crystal structures were obtained for the ligands ^{n}Bu$_4$N[HB(3-NO_2pz)(pz)$_2$] and ^{n}Bu$_4$N[HB(4-NO_2pz)(pz)$_2$] as well as for complexes

[(Tp)Fe(3-NO_2Tp)]·$(C_6H_6)_{0.5}$, [(Tp)Fe(4-NO_2Tp)], [(Tp)Fe(5-NO_2Tp)]·$(CH_3CN)_{0.5}$, [(3-NO_2Tp)$_2$Fe], [((3-NO_2)$_2$Tp)$_2$Fe], [((3-NO_2)$_2$Tp)$_2$Fe]·CH_2Cl_2, [(3-NH_2Tp)$_2$Fe] and [((3-NH_2)$_2$Tp)$_2$Fe].

All complexes display the targeted [$FeTp_2$] structure (Figures S3-12), with an octahedral Fe^{II} ion facially coordinated by two κ^3 ligands. Except for [(Tp)Fe(3-NO_2Tp)]·$(C_6H_6)_{0.5}$, [(Tp)Fe(4-NO_2Tp)] and [((3-NO_2)$_2$Tp)$_2$Fe]·CH_2Cl_2, all compounds are crystallographically centrosymmetric with the inversion center on the iron. For the monosubstituted [(Tp)Fe(5-NO_2Tp)] complex this results in a 50% occupancy disorder of the nitro group between the two ligands.

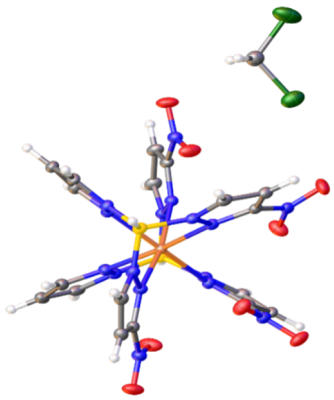

Figure 3. Single crystal structure of **[((3-NO_2)$_2$Tp)$_2$Fe]·CH_2Cl_2** drawn with anisotropic displacement ellipsoids at a 50% probability level. Fe, orange; B, yellow; C, grey; H, white; N, blue; O, red; Cl, green.

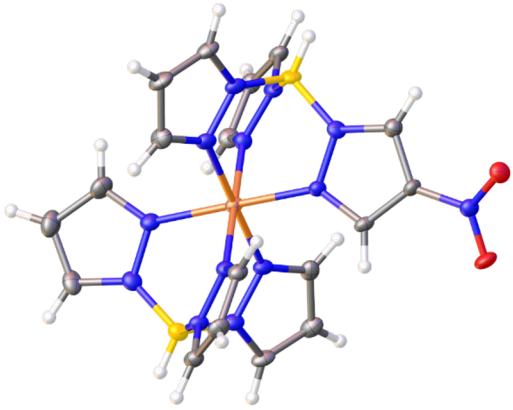

Figure 3. Single crystal structure of **[(Tp)Fe(4-NO_2Tp)]** drawn with anisotropic displacement ellipsoids at a 50% probability level. Fe, orange; B, yellow; C, grey; H, white; N, blue; O, red.

For the centrosymmetric homoleptic complex [(3-NO_2Tp)$_2$Fe], only the *trans* isomer, with substituted pyrazoles located opposite to each other across the iron center, is observed. Tetrasubstituted [(3-NO_2)$_2$Tp)$_2$Fe]·CH_2Cl_2, with its nitro groups adjacent to each other (Figure 3) is, to our knowledge, the first *cis* homoleptic complex of asymmetric trispyrazolylborate ligands

reported so far.[47, 59 60] The bending of the B-Fe-B axis from 180° to 166.9° made possible by the *cis* isomer helps accommodate the significant steric requirements of the four 3-NO_2 groups. Upon desolvation, the large orange crystals of [(3-NO_2)$_2$Tp)$_2$Fe]·CH_2Cl_2 crystals split into smaller yellow crystals. This transformation is accompanied by significant modifications in the molecular packing (Figure S17 and S18) and a change in the space group from $P2_1/c$ (one complex in the asymmetric unit, 4 complexes per cell) to *Cmce* (1/4th of a complex in the asymmetric unit, 4 complexes per cell). The departure of the CH_2Cl_2 molecules frees an estimated volume of 400Å^3 per cell[61] while the cell volume only decreases from 2910.7(3) to 2742.2(11). This added free volume allows for the molecule to adopt multiple orientations or the nitro groups while retaining a common B-Fe-B axis, resulting in the observation of fully disordered nitro groups.

The reduction of nitro groups to smaller sized amino groups results in [(3-NH_2Tp)$_2$Fe] and [(3-NH_2)$_2$Tp)$_2$Fe]. Both complexes display heavily disordered amino groups. The disorder is maximal in [(3-NH_2)$_2$Tp)$_2$Fe], which crystallizes in the $R\overline{3}$ space group: the asymmetric unit makes up only 1/6th of the complex, including a pyrazole and 2/3 of a 3-amino substituent, and the full complex is constructed by a C_3 axis along the B-Fe axis and an inversion center on the iron. In [(3-NH_2Tp)$_2$Fe], two distinct half complexes are included in the asymmetric unit, one with two-fold disorder of the amine group, one with a three-fold disorder. The disorder in both complexes is consistent with the non-participation of the 3-amino functions in intermolecular interactions: a) No hydrogen bonding is taking place in the crystals, paralleling what was observed with the 4-amino substituted complexes. [47] This points to the strong conjugation of the nitrogen lone pair into the π system of the pyrazole ring. Indeed, when hydrogen atoms can be localized in the difference Fourier map, their position correspond to a trigonal planar iminium

geometry at the nitrogen rather than a tetrahedral amine form. b) The 3-amino group, tucked in the grooves of the complex, do not participate in other types of intermolecular contacts.

The crystals of [(Tp)Fe(3-NO_2Tp)]·$(C_6H_6)_{0.5}$, [(Tp)Fe(4-NO_2Tp)], [(Tp)Fe(5-NO_2Tp)]·CH_3CN, [(3-NH_2Tp)$_2$Fe] and [((3-NH_2)$_2$Tp)$_2$Fe] are dark blue, red or purple at 100 K, suggesting they contain $S = 0$ iron(II) centers. Conversely, crystals of [(3-NO_2Tp)$_2$Fe], [((3-NO_2)$_2$Tp)$_2$Fe]·CH_2Cl_2 and [((3-NO_2)$_2$Tp)$_2$Fe] are only light yellow or orange at this temperature, pointing at a high spin state ($S = 2$). The observed Fe-N bond length confirm spin state assignments: in [(3-NO_2Tp)$_2$Fe] and [((3-NO_2)$_2$Tp)$_2$Fe] complexes they are in the range of 2.14 – 2.35 Å at 100 K, consistent with high spin Fe(II), while all other complexes have shorter Fe-N bonds [1.95 – 2.03 Å] characteristic of low spin iron (II) species.[8] Among the low spin complexes, [(Tp)Fe(3-NO_2Tp)], [(3-NH_2Tp)$_2$Fe] and [((3-NH_2)$_2$Tp)$_2$Fe] complexes have slightly larger average Fe-N bond length (1.98–1.99 Å vs. 1.96–1.97 Å for the other low spin complexes) due to the steric congestion induced by the substituents in position 3. The Fe-N bond lengths for [(3-NH_2Tp)$_2$Fe] only increase slightly from [1.975 – 1.992 Å] at 100 K to [2.009 – 2.084 Å] at room temperature, consistent with most of the complexes in the single crystal remaining low spin. The Fe-N distance for [((3-NH_2)$_2$Tp)$_2$Fe], on the other hand, increases markedly from

1.9901(9) Å to 2.1535(12) Å from 100 K to 298 K, indicating full transition to the high spin state, accompanied by a dramatic color change from dark violet to colorless.

Grandjean and coworkers identified the two distortion modes that accommodate the elongation of Fe-N bonds during spin crossover in di(trispyrazolyborate)iron complexes: twisting of the pyrazole ring, measured by an increase of the Fe-N-N-B torsion angle, and pyramidalization at the boron, marked by a decrease of the distance B-Ct(N_3) between the boron and centroid of the triangle defined by the neighboring nitrogen atoms. In the tetra-3-amino complex [(3-NH_2)$_2$Tp)$_2$Fe], pyrazole twisting does not contribute significantly (Figure 4. The Fe-N-N-B torsion angle of [((3-NH_2)$_2$Tp)$_2$Fe] is unaffected by the spin crossover between 100(2) K (red bonds) and 298(2) K (green bonds). Fe, orange B, yellow; C, grey; H, white; N, blue.): it is already present in the low spin form (Fe-N-N-B = 11.66° at 100 K), to an extend unprecedented in low spin derivatives but necessary to accommodate the 3-amino substituents, and only marginally increases in the high spin form (13.94° at 298 K). Instead, the increase in Fe-N bond

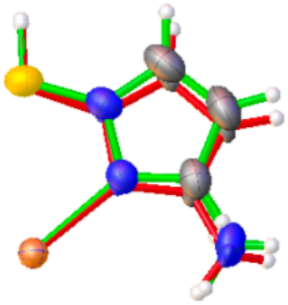

Figure 4. The Fe-N-N-B torsion angle of [((3-NH_2)$_2$Tp)$_2$Fe] is unaffected by the spin crossover between 100(2) K (red bonds) and 298(2) K (green bonds). Fe, orange B, yellow; C, grey; H, white; N, blue.

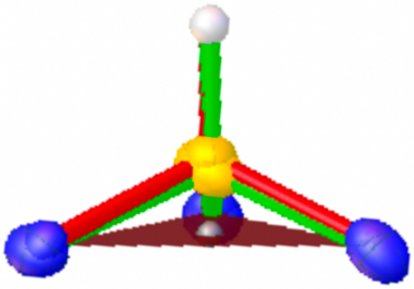

Figure 5. The spin crossover in [((3-NH_2)$_2$Tp)$_2$Fe] is accompanied by pyramidalization of the boron between 100(2) K (red bonds, LS) and 298(2) K (green bonds, HS) K (red bonds) and 298(2) K (green bonds). B, yellow; H, white; N, blue.

length is accommodated by the pyramidalization of the boron as B-Ct(N_3) decreases from 0.561 Å (LS) to 0.528 Å (HS), resulting in an increase of the ligand bite angle (Figure 5).

The packing of the complexes in the crystals, dominated by C-H…O-N and C-H…C contacts, do not display any remarkable characteristics (Figures S12-22). A complete description is provided in the Supplementary Information to this article.

Infrared spectra. The most significant feature of the IR spectra of trispyrazolylborate complexes is the B-H stretching vibration, which appears between 2452 and 2552 cm^{-1} for the compounds discussed here. The strength of the B-H bond is inversely correlated with the electronic density at the boron.[62] Thus, as expected, coordination of a ligand to the iron center draws electronic density away is drawn away from the ligand and increases the B-H wavenumber by 20 to 40 cm^{-1}. No correlation was observed between the amplitude of this shift and the spin state of the complex. Trends between the complexes give us some insight into the impact of pyrazole functionalization on the electronic density at the boron. As expected, the introduction of a nitro group on a pyrazole decreases the density at the coordinated boron, following H~3-NO_2 > 4-NO_2 ($\tilde{\nu}_{B-H}$ + 10-20 cm^{-1}) > 5-NO_2 ($\tilde{\nu}_{B-H}$ + 54 cm^{-1} from 4-NO_2) (Figure 6). Lower frequencies

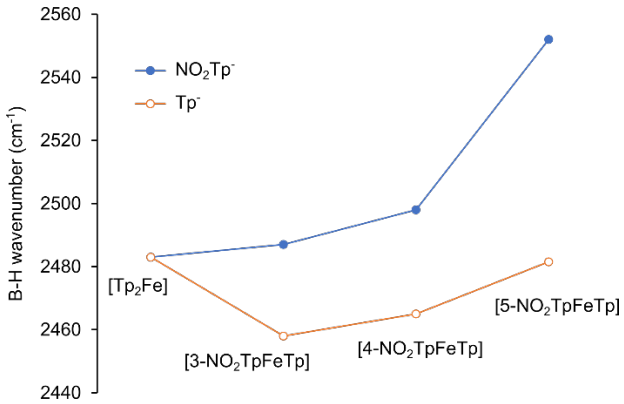

Figure 6. B-H elongation frequencies of mono-substituted nitro complexes. Line is only a guide to the eye.

for the amine-functionalized ligand are in agreement with the expected increase of electronic density at the boron, but the magnitude of the effect is smaller than that of the nitro groups. Given the symmetrical positions of the boron and iron centers with respect to the pyrazole, those electronic effects can be extrapolated to the metal, and we expect the ligand to metal σ donation to vary with the substitution as

$$3\text{-}NO_2 << 4\text{-}NO_2 << 5\text{-}NO_2 \sim H < NH_2$$

Magnetic Properties.

The temperature dependence of the susceptibility of the complexes was measured by SQUID magnetometry between 4 and 500 K. All derivatives are high spin ($S = 2$) in the high temperature limit, with $\chi_m T$ values ranging from 3.0 to 3.6 emu.K.mol^{-1} (3.8 to 4.5×10^{-5} m^3.K.mol^{-1}). The bis- and tetra-3-nitro complexes [(3-NO_2Tp)$_2$Fe] and [((3-NO_2)$_2$Tp)$_2$Fe] remain high spin at lower temperatures. The sharp decreases of the $\chi_m T$ vs. T curves (Figure 7 and Figure 8) below 40 K are consistent with a zero-field splitting of a few cm^{-1}. All other complexes display a one-step spin crossover without hysteresis (Figure 7 and Figure 8), with $T_{1/2}$ ranging from 180 to 380 K (Table 1) and various degrees of abruptness. To decouple the position and steepness of the

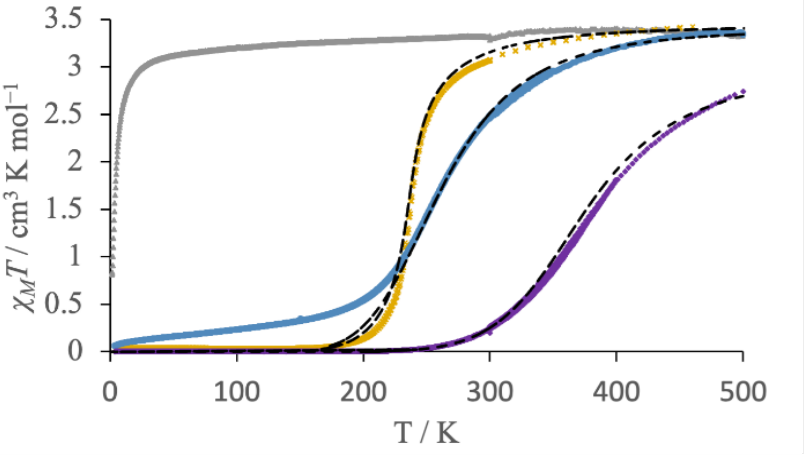

Figure 7. Temperature dependence of magnetic susceptibility of [(3-NO_2Tp)$_2$Fe] (▲), [(Tp)Fe(3-NO_2Tp)] (×), [(Tp)Fe(4-NO_2Tp)] (◆) and [(Tp)Fe(5-NO_2Tp)] (●). Dashed lines represent best fits to the Slichter-Drickamer model.

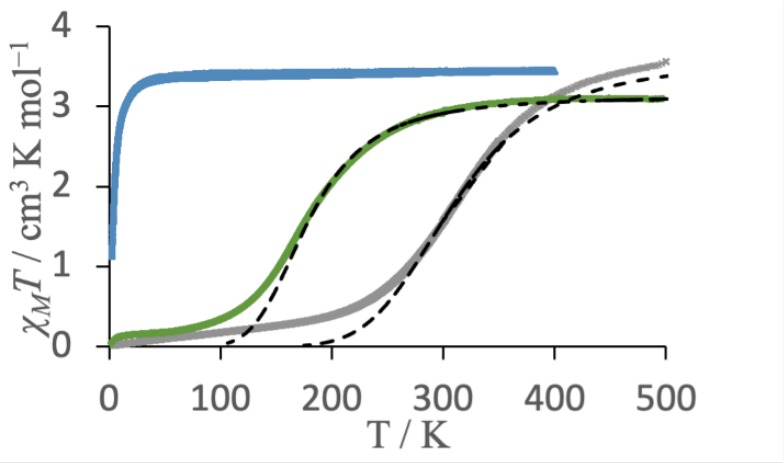

Figure 8. Temperature dependence of magnetic susceptibility of [((3-NO_2)$_2$Tp)$_2$Fe] (▲), [(3-NH_2Tp)$_2$Fe] (◆) and [((3-NH_2)$_2$Tp)$_2$Fe] (×). Dashed lines represent best fits to the Slichter-Drickamer model.

transition, the magnetic data was fitted to a regular solution model (Slichter-Drickamer model)[63, 64] which includes the enthalpy and entropy of the transition between the $S = 0$ and $S = 2$ states as well as a mixing enthalpy Γ accounting for the cooperativity of the transition. Note that those parameters are essentially empirical and should not be expected accurately represent the actual thermodynamic parameters of the spin transition. Fit parameters are summarized in Table 1.

A plot of the enthalpy of spin transition as a function of the substitution pattern shows a roughly linear increase of $\mathbf{\Delta}_r H$ with the number of electron-withdrawing 4-NO_2 substituents, and the opposite effect of electron donating 4-NH_2 groups (Figure 9, red circles). As expected, nitro groups, which enhance the π backdonation from the metal to the ligand, increase the ligand field and $\mathbf{\Delta}_r H$, while amino groups enhance ligand-to-metal π bonding, lowering the ligand field and $\mathbf{\Delta}_r H$. The deviation of 3-nitro substituted derivatives from this trend can be explained by the well-known steric effect of substituents in this position, lengthening metal-ligand bonds and favoring the high spin state. This locks the di- and tetrasubstituted 3-NO_2 derivatives in the high spin state, and lowers the enthalpy of spin transition of monosubstituted [(Tp)Fe(3-NO_2Tp)]·$(C_6H_6)_{0.5}$, by ca.

11 kJ/mol compared to the 4-substituted analogue. On the other hand, the steric requirements of the amine group appear low enough to not have a significant impact. In the absence of structural data for the desolvated [(Tp)Fe(5-NO_2Tp)] complex, we cannot, at present, explain the unexpectedly low value of $\Delta_r H$ obtained for the mono-5-nitro derivative, which from the IR data is expected to behave similarly to the unsubstituted complex. The very slow decrease of $\chi_m T$ below 220 K, marked by a deviation from the Slichter-Drikamer fit, suggests a multistep transition might be present. Looking at the cooperativity values for the compounds, and including the data previously reported for [Tp_2Fe], [(4-NH_2Tp)$_2$Fe], [(4-NO_2Tp)$_2$Fe], [((4-NO_2)$_2$Tp)FeTp] and [((4-NO_2)$_2$Tp)$_2$Fe] [35, 47], no obvious structure-property relationship was observed. It is interesting to note, however, that while most transitions are quite gradual (e.g. [((3-NH_2)$_2$Tp)$_2$Fe], [(Tp)Fe(5-NO_2Tp)]), some are remarkably abrupt (e.g. [(Tp)Fe(3-NO_2Tp)]·(C_6H_6)$_{0.5}$, [(4-NO_2Tp)$_2$Fe]), and this despite the complete lack of any specific intermolecular interaction (hydrogen bonding, π stacking etc.) in all crystal packings. One can, at best, observe a weak correlation between number of nearest neighbors of a given molecule in the crystal and the Γ value (cf. Supplementary Information).

Table 1. Slichter-Drickamer fitting parameters. Number between parentheses represent 95% confidence interval error bars

	[(Tp)Fe(3-NO_2Tp)]·(C_6H_6)$_{0.5}$	[(Tp)Fe(4-NO_2Tp)]	[(Tp)Fe(5-NO_2Tp)]	[(3-NH_2Tp)$_2$Fe]	[((3-NH_2)$_2$Tp)$_2$Fe]
$\chi_M T_{max}$	3.46	3	3.42	3.62	3.15
$T_{1/2}$ / K	238	376	262	310	182
$\Delta_r H$ / kJ mol^{-1}	13 (12.8, 13.2)	24.4 (23.7, 25.2)	17.0 (16.7,17.3)	18.5 (17.9, 19.1)	9.3 (9.2, 9.4)
$\Delta_r S$ / J mol^{-1}	54.7 (53.9, 55.5)	65.0 (63, 67)	65.0 (63.9,66.1)	59.7 (57.9, 61.6)	52.0 (45.7, 46,4)
Γ / kJ mol^{-1}	2.9 (2.8, 3.1)	1.2 (0.96, 1.48)	0 (0, 0.35)	0 (0, 0.26)	0 (0, 0.08)

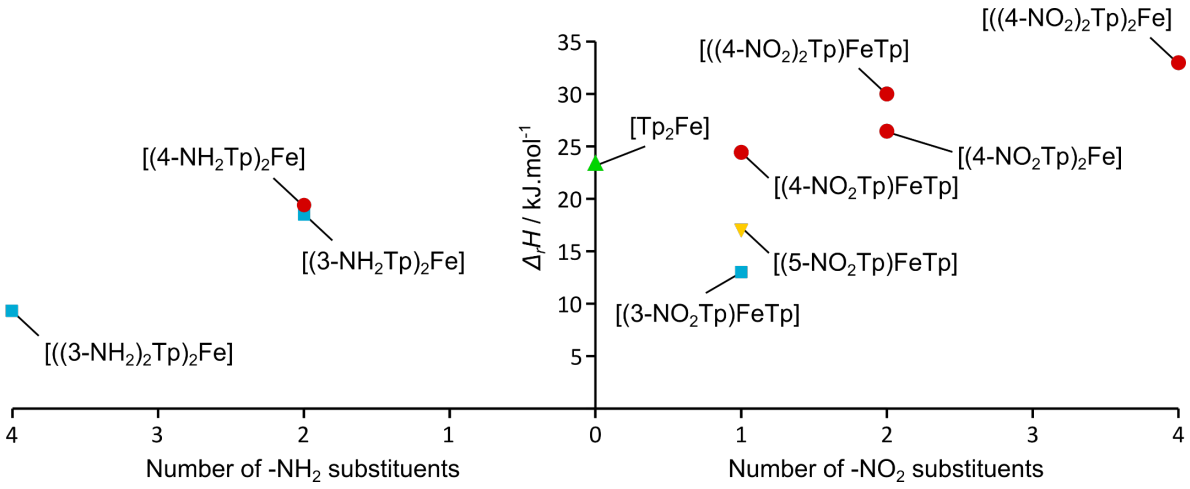

Figure 9. Enthalpy of spin transition as a function of the number of nitro or amine substituents present in position 3 (■), 4 (●) or 5 (▼) in the complex. Data for complexes [(4-NH_2Tp)$_2$Fe], [Tp$_2$Fe] (▲), [(4-NO_2Tp)$_2$Fe], [(Tp)Fe(4-NO_2Tp)] and [((4-NO_2)$_2$Tp)$_2$Fe] are taken from reference [47].

CONCLUSION

In this work, we demonstrated how the pyrazole exchange reaction could be applied to the precisely tune the functionalization of trispyrazolylborate complexes. The regioselectivity of the reaction is controlled by steric considerations, and the degree of substitution by the temperature of the reaction. Substitution patterns appear to be governed by the relative hardness of the pyrazole bases and boron centers. These observations suggest that the synthesis of multifunctional ligands should be possible by a careful selection of the order of introduction of the functionalized pyrazoles and a good control of the reaction temperature. The nitro functionalized complexes can then be reduced to the amine analogues without affecting the nature of metal cation at the core of the complex. Combined with the control in the degree of

substitution afforded by the pyrazole exchange, this yields a range of robust molecular tectons supporting a tunable number of reactive amine functions.

As expected, the di(trispyrazolylborato)iron(II) framework displays remarkably robust spin crossover properties. With the exception of highly sterically hindered di- and tetra-4 nitro substituted compounds, which are locked in a high spin configuration, all substituted complexes reported here retain their spin crossover properties. While the transition parameters of the 3-substituted derivatives is essentially governed by steric considerations, electronic effects govern complexes substituted in position 4, which display transition temperatures ranging from 70°C (diamino complex) to 130°C (tetranitro complex). The investigation of the crossover properties, however, is complicated by the cooperativity effects due to crystal packing, and some observations, in particular concerning the behavior of [(Tp)Fe(5-NO_2Tp)], remain unexplained. We expect those investigations of the spin crossover in solution, which are in progress in our laboratory, will help shedding light on those remaining questions.

ASSOCIATED CONTENT

Supporting Information

The Supporting Information is available free of charge at xxx.
Molecular structures, crystallographic parameters, crystal packing diagrams, PXRD data, IR spectra, UV-vis spectra, TGA curves, SQUID magnetization data and fits for all compounds.

Accession Codes

CCDC 2016677, 2016678, 2017277-2017281, 2018041-2018043, 2109964 and 2019476 contain the supplementary crystallographic data for this paper. These data can be obtained free of charge via www.ccdc.cam.ac.uk/data_request/cif, or by emailing data_request@ccdc.cam.ac.uk, or by

contacting The Cambridge Crystallographic Data Centre, 12 Union Road, Cambridge CB2 1EZ, UK; fax: +44 1223 336033.

AUTHOR INFORMATION

Corresponding Author

Claire Besson—Department of Chemistry, The George Washington University, 800 22nd Street NW, Washington, D.C. 20052, United States.
orcid.org/0000-0002-0502-3610;
Email: claire_besson@gwu.edu

Author

Chenyang Ma—Department of Chemistry, The George Washington University, 800 22nd Street NW, Washington, D.C. 20052, United States.
orcid.org/0000-0002-1903-1689;
Email: cma2@gwu.edu

Author Contributions

C. B. conceived the idea. C. M. conducted the experiments. C. B. and C. M. analyzed the data and wrote the manuscript.

Notes

The authors declare no competing financial interest.

ACKNOWLEDGMENTS

The authors gratefully acknowledge Prof. Cahill and Wagner (George Washington University} for the use of their X-ray diffractometers and TGA respectively. We thank Dr. J. August Ridenour and Christopher H. Hossack for their help with acquisition and treatment of the single crystal XRD data. We also thank Jordan Herder for his help with acquisition of the PXRD data.

REFERENCES

1. *Spin-Crossover Materials: Properties and Applications*, John Wiley & Sons, Ltd., 2013.
2. *Spin Crossover in Transition Metal Compounds II*, Springer-Verlag Berlin Heidelberg, 2004.
3. J. Tao, R.-J. Wei, R.-B. Huang and L.-S. Zheng, Polymorphism in spin-crossover systems, *Chemical Society Reviews*, 2012, **41**, 703-737.
4. P. D. Southon, L. Liu, E. A. Fellows, D. J. Price, G. J. Halder, K. W. Chapman, B. Moubaraki, K. S. Murray, J.-F. Létard and C. J. Kepert, Dynamic Interplay between Spin-Crossover and Host−Guest Function in a Nanoporous Metal−Organic Framework Material, *Journal of the American Chemical Society*, 2009, **131**, 10998-11009.
5. A. Bousseksou, G. Molnár, L. Salmon and W. Nicolazzi, Molecular spin crossover phenomenon: recent achievements and prospects, *Chemical Society Reviews*, 2011, **40**, 3313-3335.
6. R. J. Wei, Q. Huo, J. Tao, R. B. Huang and L. S. Zheng, Spin-crossover Fe(II)4 squares: two-step complete spin transition and reversible single-crystal-to-single-crystal transformation, *Angew Chem Int Ed Engl*, 2011, **50**, 8940-8943.
7. S. Shaik, D. Danovich, A. Fiedler, D. Schröder and H. Schwarz, Two-State Reactivity in Organometallic Gas-Phase Ion Chemistry, *Helvetica Chimica Acta*, 1995, **78**, 1393-1407.
8. P. Gütlich, A. Hauser and H. Spiering, Thermal and Optical Switching of Iron(II) Complexes, *Angewandte Chemie International Edition in English*, 1994, **33**, 2024-2054.
9. C. F. Wang, R. F. Li, X. Y. Chen, R. J. Wei, L. S. Zheng and J. Tao, Synergetic spin crossover and fluorescence in one-dimensional hybrid complexes, *Angew Chem Int Ed Engl*, 2015, **54**, 1574-1577.
10. O. Sato, Dynamic molecular crystals with switchable physical properties, *Nat Chem*, 2016, **8**, 644-656.
11. O. Kahn, J. Kröber and C. Jay, Spin Transition Molecular Materials for displays and data recording, *Advanced Materials*, 1992, **4**, 718-728.
12. O. Kahn, Spin-Transition Polymers: From Molecular Materials Toward Memory Devices, *Science*, 1998, **279**, 44-48.
13. K. Senthil Kumar and M. Ruben, Emerging trends in spin crossover (SCO) based functional materials and devices, *Coordination Chemistry Reviews*, 2017, **346**, 176-205.
14. S. M. Fatur, S. G. Shepard, R. F. Higgins, M. P. Shores and N. H. Damrauer, A Synthetically Tunable System To Control MLCT Excited-State Lifetimes and Spin States in Iron(II) Polypyridines, *J Am Chem Soc*, 2017, **139**, 4493-4505.
15. C. Bartual-Murgui, S. Vela, M. Darawsheh, R. Diego, S. J. Teat, O. Roubeau and G. Aromí, A probe of steric ligand substituent effects on the spin crossover of Fe(ii) complexes, *Inorganic Chemistry Frontiers*, 2017, **4**, 1374-1383.
16. H.-J. Lin, D. Siretanu, D. A. Dickie, D. Subedi, J. J. Scepaniak, D. Mitcov, R. Clérac and J. M. Smith, Steric and Electronic Control of the Spin State in Three-Fold Symmetric, Four-Coordinate Iron(II) Complexes, *Journal of the American Chemical Society*, 2014, **136**, 13326-13332.
17. J. Fleisch, P. Gütlich, K. Hasselbach and W. Müller, HIGH SPIN-LOW SPIN TRANSITION IN SUBSTITUTED PHENANTHROLINE COMPLEXES OF IRON (II), *Journal de Physique Colloques*, 1974, **35**, C6-659-C656-662.

18. J. M. Holland, S. A. Barrett, C. A. Kilner and M. A. Halcrow, Control of the spin state of Fe(II) 2,6-di(pyrazol-1-yl)pyridine complexes by distal ligand substitution, *Inorganic Chemistry Communications*, 2002, **5**, 328-332.
19. J. Elhaïk, D. J. Evans, C. A. Kilner and M. A. Halcrow, A structural, magnetic and Mössbauer spectroscopic study of an unusual angular Jahn–Teller distortion in a series of high-spin iron(ii) complexes, *Dalton Transactions*, 2005, DOI: 10.1039/B502175H, 1693-1700.
20. A. Santoro, L. J. Kershaw Cook, R. Kulmaczewski, S. A. Barrett, O. Cespedes and M. A. Halcrow, Iron(II) Complexes of Tridentate Indazolylpyridine Ligands: Enhanced Spin-Crossover Hysteresis and Ligand-Based Fluorescence, *Inorganic Chemistry*, 2015, **54**, 682-693.
21. A. Kimura and T. Ishida, Spin-Crossover Temperature Predictable from DFT Calculation for Iron(II) Complexes with 4-Substituted Pybox and Related Heteroaromatic Ligands, *ACS Omega*, 2018, **3**, 6737-6747.
22. A. Kimura and T. Ishida, Pybox-Iron(II) Spin-Crossover Complexes with Substituent Effects from the 4-Position of the Pyridine Ring (Pybox = 2,6-Bis(oxazolin-2-yl)pyridine), *Inorganics*, 2017, **5**.
23. L. J. Kershaw Cook, R. Kulmaczewski, R. Mohammed, S. Dudley, S. A. Barrett, M. A. Little, R. J. Deeth and M. A. Halcrow, A Unified Treatment of the Relationship Between Ligand Substituents and Spin State in a Family of Iron(II) Complexes, *Angew Chem Int Ed Engl*, 2016, **55**, 4327-4331.
24. J. G. Park, I.-R. Jeon and T. D. Harris, Electronic Effects of Ligand Substitution on Spin Crossover in a Series of Diiminoquinonoid-Bridged FeII2 Complexes, *Inorganic Chemistry*, 2015, **54**, 359-369.
25. K. Nakano, N. Suemura, K. Yoneda, S. Kawata and S. Kaizaki, Substituent effect of the coordinated pyridine in a series of pyrazolato bridged dinuclear diiron(ii) complexes on the spin-crossover behavior, *Dalton Transactions*, 2005, DOI: 10.1039/B416986G, 740-743.
26. G. J. Long and B. B. Hutchinson, Spin equilibrium in iron(II) poly(1-pyrazolyl)borate complexes: low-temperature and high-pressure Moessbauer spectral studies, *Inorganic Chemistry*, 1987, **26**, 608-613.
27. S. Calogero, G. G. Lobbia, P. Cecchi, G. Valle and J. Friedl, A Mössbauer study of some iron(II) and iron(III) poly(pyrazolyl)borates. The x-ray crystal structures of iron(II)bis[hydridotris(3-methyl-1H-pyrazol-1-yl)borate] and iron(II)bis[hydridotris(1H-pyrazol-1-yl)borate] tetrafluoroborate, *Polyhedron*, 1994, **13**, 87-97.
28. P. Cecchi, M. Berrettoni, M. Giorgetti, G. Gioia Lobbia, S. Calogero and L. Stievano, The effect of the 3-trifluoromethyl substituent in polypyrazolylborato complexes on the iron(II) spin state; X-ray diffraction and absorption and Mössbauer studies, *Inorganica Chimica Acta*, 2001, **318**, 67-76.
29. M. Cavallini, Status and perspectives in thin films and patterning of spin crossover compounds, *Physical Chemistry Chemical Physics*, 2012, **14**, 11867-11876.
30. J. P. Jesson, S. Trofimenko and D. R. Eaton, Spin equilibria in octahedral iron(II) poly((1-pyrazolyl)-borates, *Journal of the American Chemical Society*, 1967, **89**, 3158-3164.
31. S. Trofimenko, Boron-pyrazole chemistry. II. Poly(1-pyrazolyl)-borates, *Journal of the American Chemical Society*, 1967, **89**, 3170-3177.

32. T. Zhao, I. Boldog, V. Spasojevic, A. Rotaru, Y. Garcia and C. Janiak, Solvent-triggered relaxative spin state switching of [Fe(HB(pz)3)2] in a closed nano-confinement of NH2-MIL-101(Al), *Journal of Materials Chemistry C*, 2016, **4**, 6588-6601.
33. T. Mahfoud, G. Molnár, S. Cobo, L. Salmon, C. Thibault, C. Vieu, P. Demont and A. Bousseksou, Electrical properties and non-volatile memory effect of the [Fe(HB(pz)3)2] spin crossover complex integrated in a microelectrode device, *Applied Physics Letters*, 2011, **99**.
34. F. Grandjean, G. J. Long, B. B. Hutchinson, L. Ohlhausen, P. Neill and J. D. Holcomb, Study of the high-temperature spin-state crossover in the iron(II) pyrazolylborate complex Fe[HB(pz)3]2, *Inorganic Chemistry*, 1989, **28**, 4406-4414.
35. L. Salmon, G. Molnár, S. Cobo, P. Oulié, M. Etienne, T. Mahfoud, P. Demont, A. Eguchi, H. Watanabe, K. Tanaka and A. Bousseksou, Re-investigation of the spin crossover phenomenon in the ferrous complex [Fe(HB(pz)3)2], *New Journal of Chemistry*, 2009, **33**.
36. N. Tsuchiya, A. Tsukamoto, T. Ohshita, T. Isobe, M. Senna, N. Yoshioka and H. Inoue, Stress-induced ligand field distribution and consequent multi-mode spin crossover in $Fe^{II}(phen)_2(NCS)_2$ and $Fe^{II}[HB(pz)_3]_2$, *Sol. State Sci.*, 2001, **3**, 705-714.
37. D. L. Reger, J. R. Gardinier, J. D. Elgin, M. D. Smith, D. Hautot, G. J. Long and F. Grandjean, Structure−Function Correlations in Iron(II) Tris(pyrazolyl)borate Spin-State Crossover Complexes, *Inorganic Chemistry*, 2006, **45**, 8862-8875.
38. G. J. Long, F. Grandjean and D. L. Reger, in *Spin Crossover in Transition Metal Compounds I*, eds. P. Gütlich and H. A. Goodwin, Springer Berlin Heidelberg, Berlin, Heidelberg, 2004, DOI: 10.1007/b13530, pp. 91-122.
39. P. Hamon, J.-Y. Thépot, M. Le Floch, M.-E. Boulon, O. Cador, S. Golhen, L. Ouahab, L. Fadel, J.-Y. Saillard and J.-R. Hamon, Dramatic Remote Substitutent Effects on the Electronic Spin State of Bis(scorpionate) Iron(II) Complexes, *Angew. Chem. Int. Ed.*, 2008, **47**, 8687-8691.
40. D. L. Reger, J. R. Gardinier, M. D. Smith, A. M. Shahin, G. J. Long, L. Rebbouh and F. Grandjean, Polymorphism in $Fe[(p\text{-}IC_6H_4)B(3\text{-}Mepz)_3]_2$(pz = Pyrazolyl): Impact of Supramolecular Structure on an Iron(II) Electronic Spin-State Crossover, *Inorg. Chem.*, 2005, **44**, 1852-1866.
41. D. L. Reger, J. R. Gardinier, W. R. Gemmill, M. D. Smith, A. M. Shahin, G. J. Long, L. Rebbouh and F. Grandjean, Formation of Third Generation Poly(pyrazolyl)borate Ligands from Alkyne Coupling Reactions of $Fe[(p\text{-}IC_6H_4)B(3\text{-}Rpz)_3]_2$(R = H, Me; pz = Pyrazolyl): Pathways toward Controlling an Iron(II) Electronic Spin-State Crossover, *J. Am. Chem. Soc.*, 2005, **127**, 2303-2316.
42. V. Davesne, M. Gruber, T. Miyamachi, V. D. Costa, S. Boukari, F. Scheurer, L. Joly, P. Ohresser, E. Otero, F. Choueikani, A. B. Gaspar, J. A. Real, W. Wulfhekel, M. Bowen and E. Beaurepaire, First glimpse of the soft X-ray induced excited spin-state trapping effect dynamics on spin cross-over molecules, *J. Chem. Phys.*, 2013, **139**, 074708.
43. Y. Sohrin, H. Kokusen and M. Matsui, Control of Ligand Field Strength through Intra- and Interligand Contact. Octahedral Iron(II) Poly(pyrazolyl)borate Complexes, *Inorg. Chem.*, 1995, **34**, 3928-3934.
44. C. Janiak, S. Temizdemir, S. Dechert, W. Deck, F. Girgsdies, J. Heinze, Mario J. Kolm, Tobias G. Scharmann and Oliver M. Zipffel, Binary [Hydrotris(indazol-1-yl)borato]metal Complexes, $M(Tp_4Bo)_2$ with M = Fe, Co, Ni, Cu, and Zn: Electronic Properties and

Solvent-Dependent Framework Structures through C−H···π Interactions, *Eur. J. Inorg. Chem.*, 2000, **2000**, 1229-1241.
45. T. Buchen and P. Gütlich, Substituent effects on the spin equilibrium in iron(II) pyrazolylborate complexes, *Inorg. Chim. Acta*, 1995, **231**, 221-223.
46. F. Remacle, F. Grandjean and G. J. Long, A Density Functional Theory Calculation of the Electronic Properties of Several High-Spin and Low-Spin Iron(II) Pyrazolylborate Complexes, *Inorg. Chem.*, 2008, **47**, 4005-4014.
47. H. Flototto, T. Secker, P. Kogerler and C. Besson, Amine-Functionalized Spin Crossover Building Blocks, *Eur J Inorg Chem*, 2019, **2019**, 4621-4624.
48. R. Hüttel and F. Büchele, ÜberN-Nitro-pyrazole, *Chemische Berichte*, 1955, **88**, 1586-1590.
49. E. Nageswara Rao, P. Ravi, S. P. Tewari and S. Venugopal Rao, Experimental and theoretical studies on the structure and vibrational properties of nitropyrazoles, *Journal of Molecular Structure*, 2013, **1043**, 121-131.
50. N. V. Latypov, V. A. Silevich, P. A. Ivanov and M. S. Pevzner, Diazotization of aminonitropyrazoles, *Chemistry of Heterocyclic Compounds*, 1976, **12**, 1355-1359.
51. S. Ek and N. V. Latypov, Four Syntheses of 4-Amino-3,5-dinitropyrazole, *Journal of Heterocyclic Chemistry*, 2014, **51**, 1621-1627.
52. J. R. Bour, N. M. Camasso and M. S. Sanford, Oxidation of Ni(II) to Ni(IV) with Aryl Electrophiles Enables Ni-Mediated Aryl-CF3 Coupling, *J Am Chem Soc*, 2015, **137**, 8034-8037.
53. I. G. R. Gutz, CurTiPot 4.3.0.).
54. O. S. Attaryan, A. O. Baltayan, K. S. Badalyan, G. G. Minasyan and S. G. Matsoyan, Cyanoethylation of pyrazoles under conditions of phase-transfer catalysis and hydrogenation of the cyanoethylation products, *Russ J Gen Chem+*, 2006, **76**, 1131-1133.
55. M. F. Hawthorne and W. L. Budde, Nucleophilic substitution at tetrahedral boron. Trimethyl- and triethylamine-borone substrates, *J. Am. Chem. Soc.*, 1971, **93**, 3147-3150.
56. S. Toyota, T. Futawaka, M. Asakura, H. Ikeda and M. Ōki, Experimental and Theoretical Evidence of an S_N2-Type Mechanism for Dissociation of B−N Coordination Bonds in 2,6-Bis((dimethylamino)methyl)phenylborane Derivatives, *Organometallics*, 1998, **17**, 4155-4163.
57. J. A. Menéndez, A. Arenillas, B. Fidalgo, Y. Fernández, L. Zubizarreta, E. G. Calvo and J. M. Bermúdez, Microwave heating processes involving carbon materials, *Fuel Processing Technology*, 2010, **91**, 1-8.
58. E. Cini, E. Petricci and M. Taddei, Pd/C Catalysis under Microwave Dielectric Heating, *Catalysts*, 2017, **7**.
59. D. J. Darensbourg, E. L. Maynard, M. W. Holtcamp, K. K. Klausmeyer and J. H. Reibenspies, Synthesis and X-ray Structure of the Novel Aluminum Complex [{η3-HB(3-Phpz)2(5-Phpz)}2Al][AlCl4]. Catalysis of CO2/Propylene Oxide to Propylene Carbonate by the AlCl4- Anion, *Inorganic Chemistry*, 1996, **35**, 2682-2684.
60. S. Trofimenko, J. C. Calabrese, P. J. Domaille and J. S. Thompson, Steric effects in polypyrazolylborate ligands. Poly(3-isopropylpyrazolyl)borates: ligands of intermediate steric requirements, *Inorganic Chemistry*, 1989, **28**, 1091-1101.
61. (volume of one molecule estimated at 106 Å 3 from density at RT, 96 Å 3 at -57oC) but cell (Z=4 in both cases)

62. T. T. Chin, S. R. Lovelace, W. E. Geiger, C. M. Davis and R. N. Grimes, Infrared Spectroelectrochemistry of Boron-Hydrogen Stretches: A Tool for Diagnosis of Delocalization in Mixed-Valent Metallacarborane Complexes, *Journal of the American Chemical Society*, 1994, **116**, 9359-9360.
63. C. P. Slichter and H. G. Drickamer, Pressure-Induced Electronic Changes in Compounds of Iron, *The Journal of Chemical Physics*, 1972, **56**, 2142-2160.
64. M. Sorai, M. Nakano and Y. Miyazaki, Calorimetric investigation of phase transitions occurring in molecule-based magnets, *Chem Rev*, 2006, **106**, 976-1031.